THE JOURNAL OF BIOLOGICAL CHEMISTRY
© 1984 by The American Society of Biological Chemists, Inc.

Vol. 259, No. 10, Issue of May 25, pp. 6472-6480, 1984
Printed in U.S.A.

Chloride Binding to the Anion Transport Binding Sites of Band 3

A ^{35}Cl NMR STUDY*

(Received for publication, September 13, 1983)

Joseph J. Falke‡, R. J. Pace§, and Sunney I. Chan¶

From the Arthur Amos Noyes Laboratory of Chemical Physics, California Institute of Technology, Pasadena, California 91125

Band 3 is an integral membrane protein that exchanges anions across the red cell membrane. Due to the abundance and the high turnover rate of the band 3 transport unit, the band 3 system is the most heavily used ion-transport system in a typical vertebrate organism. Here we show that ^{35}Cl NMR enables direct and specific observation of substrate Cl^- binding to band 3 transport sites, which are identified by a variety of criteria: (*a*) the sites are inhibited by 4,4′-dinitrostilbene-2,2′-disulfonate, which is known to inhibit competitively Cl^- binding to band 3 transport sites; (*b*) the sites have affinities for 4,4′-dinitrostilbene-2,2′-disulfonate and Cl^- that are quantitatively similar to the known affinities of band 3 transport sites for these anions; and (*c*) the sites have relative affinities for Cl^-, HCO_3^-, F^-, and I^- that are quantitatively similar to the known relative affinities of band 3 transport sites for these anions. The ^{35}Cl NMR assay also reveals a class of low affinity Cl^- binding sites ($K_D \gg 0.5$ M) that are not affected by 4,4′-dinitrostilbene-2,2′-disulfonate. These low affinity sites may be responsible for the inhibition of band 3 catalyzed anion exchange that has been previously observed at high [Cl^-]. In the following paper the ^{35}Cl NMR assay is used to resolve the band 3 transport sites on opposite sides of the membrane, thereby enabling direct observation of the transmembrane recruitment of transport sites.

Band 3 is an integral membrane protein in human erythrocyte membranes. The protein consists of a single polypeptide chain (M_r = 95,000) and although the catalytic unit is thought to be the monomer (1), the protein exists in the membrane as a dimer (2). Band 3 has at least two functions, one structural and the other physiological. The cytoplasmic portion of this protein contains the site to which the red cell cytoskeleton binds and thereby is anchored to the membrane (3, 4). Completely unrelated to this structural function is the role of band 3 in the respiratory system, where it facilitates the transport of CO_2 by the bloodstream. As the central component of the Hamburger (or chloride) shift, band 3 exchanges HCO_3^-, which is produced from CO_2 and H_2O by carbonic anhydrase inside the cell, for Cl^- on the other side of the membrane (5–7). This exchange process allows the serum to carry the bulk of the dissolved CO_2 in the form of HCO_3^-. The physiological importance of this exchange process is illustrated by the fact that the band 3 system is the most heavily used ion-transport system in a typical vertebrate animal such as man ("Appendix I").[1] We believe that an important current goal of membrane biochemistry should be to understand, in molecular terms, the anion transport event which occurs within this relatively simple and easily obtainable band 3 protein.

The mechanism of band 3-catalyzed anion exchange has been extensively studied in kinetic experiments; for a review, see Ref. 1. These kinetic studies have stimulated the development of a variety of models (1, 8–15) for the exchange process, all of which postulate the existence of one or more transport sites that bind substrate anion during the transport event. The existence of transport sites is suggested by the saturation kinetics that are observed at high concentrations of substrate anion (1); however, saturation kinetics are also exhibited by ion channels that require single file passage of ions (16). Thus, we have attempted to observe directly transport sites using an assay for substrate (chloride) binding to band 3.

Chloride binding to protein binding sites has been studied in a large number of water-soluble protein systems using ^{35}Cl NMR, and the theory and practice of this approach have been the subject of extensive reviews by Lindman and Forsén (17) and Forsén and Lindman (18). Rothstein and his co-workers (19) first showed that ^{35}Cl NMR can be used to study the binding of chloride to band 3; we have improved upon this technique and extended its applications in the two papers presented here. In the first paper we use the ^{35}Cl NMR chloride binding assay to observe two classes of chloride binding sites on leaky red cell membranes. One class is composed of low affinity sites that may include nonspecific chloride binding sites, while the other class is composed of high affinity chloride binding sites. We are able to identify the high affinity sites as band 3 transport sites by studying their affinity for a variety of anions: chloride, fluoride, iodide, and bicarbonate, as well as the inhibitor of anion exchange DNDS.[2] Surprisingly, we see no evidence of an inhibitory chloride binding site termed the modified site (20) which has

* This work was supported by National Institute of General Medical Sciences Grant GM-22432. Contribution 6887 from the Arthur Amos Noyes Laboratory of Chemical Physics, California Institute of Technology, Pasadena, CA 91125. The costs of publication of this article were defrayed in part by the payment of page charges. This article must therefore be hereby marked "*advertisement*" in accordance with 18 U.S.C. Section 1734 solely to indicate this fact.

‡ Supported by a National Science Foundation Predoctoral Fellowship.

§ Present address, Research School of Chemistry, Australian National University, P. O. Box 4, Canberra, A.C.T. 2600, Australia.

¶ To whom correspondence should be addressed.

[1] Appendices I–III (including Figs. A1 and A2) are presented in miniprint at the end of this paper. Miniprint is easily read with the aid of a standard magnifying glass. Full size photocopies are available from the Journal of Biological Chemistry, 9650 Rockville Pike, Bethesda, MD 20814. Request Document No. 83M-2651, cite the authors, and include a check or money order for $5.60 per set of photocopies. Full size photocopies are also included in the microfilm edition of the Journal that is available from Waverly Press.

[2] The abbreviation used is: DNDS, 4,4′-dinitrostilbene-2,2′-disulfonate.

been thought to be present on band 3. In the second paper (21) we (*a*) resolve the transport sites into two populations on opposite membrane surfaces, (*b*) study the transmembrane recruitment of band 3 transport sites, and (*c*) discuss the implications of these studies for the mechanism of band 3 catalyzed chloride exchange.

MATERIALS AND METHODS

Reagents—4,4′-Dinitrostilbene-2,2′-disulfonic acid, disodium salt (Pfaltz and Bauer), was recrystallized one time as follows: 10 g of DNDS were dissolved in 200 ml of boiling H_2O, 100 ml of saturated NaCl in H_2O (24 °C) were added, the suspension was cooled (4 °C) overnight, and the crystals were isolated and washed with 60% saturated NaCl in H_2O (0 °C). When the crystals were redissolved in H_2O, they gave a single absorption maximum at 353 nm and the A_{353}/A_{310} ratio was 2.25, indicating pure or nearly pure *trans*-isomer (22). Used without further purification were: D_2O (Aldrich), phenylmethylsulfonyl fluoride (Sigma), and dithiothreitol (Calbiochem-Behring). All other chemicals used were reagent grade or better.

Preparation of Ghost Membranes—Freshly outdated human blood (packed red cells) was a kind gift of the Los Angeles Chapter of the American Red Cross. Two units of any type were mixed and ghost membranes were prepared essentially as described previously (23, 24). The following modifications were necessary to produce large quantities of leaky ghost membranes (~100 ml of pellet) which were not crushed by the forces of centrifugation (see Ref. 21). The entire preparation was carried out at 0 to 4 °C using a Sorvall GSA rotor, and the efficiency of all washes was maximized by filling the centrifuge bottles to maximum capacity. The packed red cells were aliquoted into six 250-ml centrifuge bottles and suspended in PBS (150 mM NaCl, 10 mM NaH_2PO_4, pH to 8 with NaOH). The cells were pelleted by centrifugation at 8,000 rpm (10,400 × g_{max}) for 20 min, then the supernatant and buffy coat were removed by aspiration. The cells were washed twice more by resuspending each time in phosphate-buffered saline, then pelleting (10 min at 3,000 rpm or 1,500 × g_{max}), and then aspirating away the supernatant. Following the washes, the cells were lysed. The pellets were resuspended in 5P8(+) (or 5 mM NaH_2PO_4, pH to 8 with NaOH, 130 μM dithiothreitol, and 10 μM phenylmethylsulfonyl fluoride) then the membranes were pelleted by centrifugation at 11,000 rpm (19,700 × g_{max}) for 20 min. The supernatant and the dense pellet underlying the membranes were removed by aspiration. This wash cycle in 5P8(+) was repeated six or seven times until the supernatant was colorless. The resulting leaky ghost membranes possess the typically observed range of shapes from biconcave to spherical, and few (~5%) crushed ghosts are produced (see Ref. 21). The membranes were used within 4 days and were stored at 4 °C.

NMR Sample Preparation—In all experiments samples were made on ice by diluting the ghost membrane pellet from the above preparation with an equal volume of ice-cold 2 × NMR buffer (see figure and table legends for final buffer compositions). Samples that were compared to each other, for instance those plotted in the same figure, were always made using aliquots of the same membrane suspension. Samples were always prepared and stored on ice and were assayed using ^{35}Cl NMR the same day, within 10 h of preparation.

For experiments with added DNDS, a sufficiently large volume of ghosts in NMR buffer was aliquoted to give identical samples, then an appropriate volume of inhibitor (in H_2O) stock solution was added to each sample to give the desired final inhibitor concentration. The same total volume (50 μl/ml of sample) of inhibitor stock plus H_2O was added to all the related samples so that they were identical except (when appropriate) for the inhibitor concentration. Due to the light-sensitive nature of DNDS, the DNDS stock solution was stored in darkness and was used only if it satisfied the conditions $A_{353}/A_{310} \geq 2.20$ (or, more than 95% *trans*-isomer, the *cis*-isomer being inactive (22)). Also, for routine assays excess DNDS (1.0 mM total, which gives ~0.9 mM unbound) was used so that full inhibition of the DNDS-sensitive line broadening was ensured even if some degradation occurred.

Samples containing different amounts of the anions chloride, bicarbonate, fluoride, or iodide (Figs. 5 and 6) were prepared by diluting 1 volume of membranes with 1 volume of a different 2 × NMR buffer stock for each anion concentration. The ionic strength was held constant in all samples by including a sufficient amount of citric acid (pH to 8.0 with NaOH). Thus, enough citrate was added to make the ionic strength the same as that of the sample containing the highest concentration (500 mM, Fig. 5, or 200 mM, Fig. 6) of the varying anion. No citrate was added to the latter sample.

^{35}Cl NMR Spectroscopy—The spectra were obtained using one of two NMR spectrometers: a JEOL FX-90 (^{35}Cl resonance frequency is 8.8 MHz) or a Varian XL-200 (^{35}Cl resonance frequency is 19.6 MHz). The standard parameters for spectral acquisition were as follows. The spectral width was 1000 Hz, containing 256 data points and centered on the solution chloride peak in the ^{35}Cl NMR spectrum. Using 5- or 10-mm sample tubes, from 1000 to 3000 pulses were accumulated for up to 6.4 min (3000 pulses) at 3 °C without sample spinning. An extra linebroadening of precisely 10.0 Hz was added to all samples during data processing to improve signal/noise, and the number of Fourier transform points was zero filled to over 8000 to smooth the spectrum (see Ref. 25). The central 500 Hz of the spectrum was plotted and the line width of the ^{35}Cl peak at half-height hand measured. For all experiments the same acquisition parameters were used for samples that were compared to each other, for instance, those plotted in the same figure.

NMR Sample Analysis—After NMR spectra were obtained, samples were stored overnight at 4 °C before chemical analysis. Total ghost protein was determined using the modified (26) Lowry protein assay (27) that has been developed for use with membrane samples. The concentration of nonmembrane-bound DNDS was determined essentially as described elsewhere (28, 29). The membranes were pelleted by centrifugation for 45 min at 15,000 rpm (29,000 × g_{max}) in a Sorvall SS-34 rotor, 3-ml tubes. The optical absorbance of the supernatant was measured and corrected for the background absorbance present in supernatants containing no inhibitor. The DNDS concentration was calculated using the molar extinction coefficient $\epsilon_{353} = 3.0 \times 10^4$ (22).

Statistics—All confidence limits for means and for best fit (nonlinear least squares) parameters are given as ± one S.D. for $n \geq 3$.

RESULTS

The $^{35}Cl^-$ NMR Resonance—For chloride in aqueous solution, the chloride ^{35}Cl NMR spectrum (here termed the $^{35}Cl^-$ NMR spectrum) contains a single resonance of Lorentzian shape (Figs. 1 and 2). Within experimental error, the shape of the observed resonance remains Lorentzian when leaky ghost membranes are added (Figs. 1 and 2). Note, however, that the line width at half-height of the resonance is increased by the membranes (Fig. 1). This line width increase is due to the presence of membrane-bound chloride binding sites. In the following, the line width increase will be used as an assay for these sites; but first it is necessary to (*a*) examine the characteristics of the $^{35}Cl^-$ NMR spectrum and (*b*) demonstrate the validity of the binding site assay in the leaky ghost system.

Identity of the Chloride Ions that Give Rise to the Observed $^{35}Cl^-$ NMR Resonance—At a given instant in time, the chloride ions in a suspension of ghost membranes can be divided into three populations: chloride ions in the extracellular so-

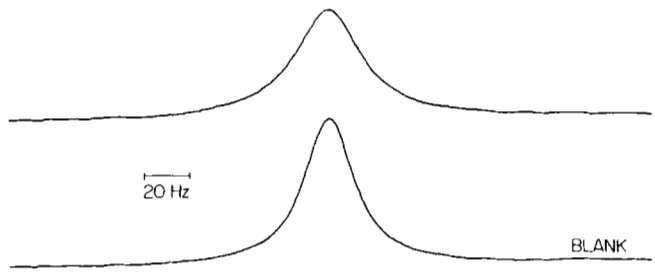

FIG. 1. **The effect of ghost membranes on the $^{35}Cl^-$ NMR spectrum.** Shown are typical spectra obtained at 19.6 MHz and 3 °C using standard $^{35}Cl^-$ line broadening assay parameters (see text). *Upper spectrum*, with leaky ghost membranes, 1.4 mg/ml of total ghost protein. *Lower spectrum*, without ghost membranes. The line widths at half-height are 34.5 and 27.1 Hz for the *upper* and *lower* spectra, respectively. Each sample contained: 250 mM NH_4Cl, 5 mM NaH_2PO_4, 20% D_2O, pH to 8.0 with NH_4OH. The two spectra are plotted at the same absolute intensity.

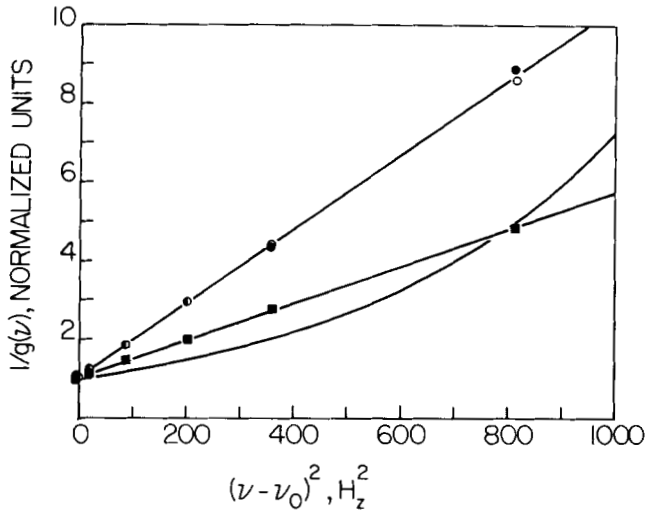

FIG. 2. **The line shape of the $^{35}Cl^-$ NMR spectra.** Spectra for samples containing leaky ghosts (■), ghosts plus 1% sodium dodecyl sulfate (●), and no ghosts (○) were normalized so that the absorption intensity ($g(\nu_0)$) of each spectrum at the resonance frequency (ν_0) was 1. Then the absorption intensity ($g(\nu)$) at other frequencies (ν) was measured and the inverse of the absorption intensity ($1/g(\nu)$) was recorded in this plot which linearizes Lorentzian spectra. The *solid lines* are nonlinear least squares best fit curves. The *straight lines* show the best fit Lorentzian line shapes and the *curved line* shows the best fit Gaussian line shape for the ghost (■) points. The buffer was: 250 mM NaCl, 5 mM NaH_2PO_4, 20% D_2O, pH to 8.0 with NaOH. Spectral parameters were 19.6 MHz, 3 °C and standard assay parameters (see text).

lution, chloride ions in the intracellular solution, and chloride ions bound to the membranes. The Lorentzian shape of the observed $^{35}Cl^-$ resonance indicates that the resonance stems from a homogeneous population of chloride ions. This homogeneous population contains 100 ± 2% of the total number of chloride ions in the sample (from integration of the spectra used to generate Fig. 2). Thus, the observed population is large compared to the population of chloride bound to macromolecules (total protein ≤10 μM, observed chloride 250 ± 5 mM), and it follows that the bulk of the observed population are solution choride ions.

Both the intracellular and extracellular populations of solution chloride contribute to the observed $^{35}Cl^-$ resonance. The ratio of intracellular:extracellular chloride ions in these samples is ~25:75 (calculated assuming 100 μm^3 total volume and 6×10^{-10} mg of total protein/ghost membrane). The integration data indicate that the majority of chloride ions in both compartments are visible. The fact that these two populations give rise to a $^{35}Cl^-$ resonance due to a homogeneous population of chloride ions is not surprising, since large holes exist in these leaky ghost membranes ((30); see also Ref. 21). These holes should allow rapid exchange of chloride ions between the intra- and extracellular compartments such that the intra- and extracellular solution chloride ions are chemically equivalent on the NMR timescale. Thus, the $^{35}Cl^-$ NMR resonance of samples that contain ghost membranes is best described as the spectrum of a homogeneous population of solution chloride ions whose line width is perturbed (increased) by the presence of chloride binding sites.

Further Analysis of the Observed $^{35}Cl^-$ Resonance—Two characteristics of the observed $^{35}Cl^-$ NMR spectrum deserve further explanation. First, the shape of the observed spectrum is simple, despite the fact that the ^{35}Cl nucleus ($S = 3/2$) actually gives rise to three distinct NMR transitions. Second, the increase in line width caused by ghost membranes is of interest because this effect forms the basis of the assay for chloride binding sites used here.

Both the shape and the width of the $^{35}Cl^-$ spectrum are largely controlled by the effect of the quadrupolar interaction on the three $^{35}Cl^-$ NMR transitions. The ^{35}Cl nucleus possesses an electric quadrupole moment, which interacts with the electric field gradient in the nucleus. The magnitude of this field gradient is large when the chloride ion's electron cloud is polarized by an asymmetrical ligand environment. However, the effect of the field gradient on the $^{35}Cl^-$ NMR spectrum is decreased when the chloride-ligand complex tumbles sufficiently rapidly to partially or completely randomize the direction of the field gradient.

The tumbling of hydrated chloride in aqueous solution is unrestricted, essentially isotropic and rapid. Under these conditions the quadrupolar interaction is averaged to zero and the three $^{35}Cl^-$ NMR transitions have identical resonance frequencies and line widths so that they sum to give a Lorentzian absorption (Figs. 1 and 2). In contrast, a large quadrupolar interaction occurs when chloride binds to a slowly tumbling, asymmetric binding site on a macromolecule. The large quadrupolar interaction causes differences in the resonance frequencies and line widths of the three transitions so that the spectrum is no longer Lorentzian. However, in the experiments presented here, free chloride in solution is present in large molar excess relative to chloride bound to macromolecules. Thus, the solution chloride spectrum with its Lorentzian shape dominates the observed spectrum, even in the presence of ghost membranes (Figs. 1 and 2).

The increase in the line width of the $^{35}Cl^-$ NMR resonance in the presence of ghost membranes is due to the exchange of chloride between solution and chloride binding sites associated with the membranes (Fig. 1). Due to the quadrupolar interaction and to shifts of resonance frequencies that occur upon binding, the line width of a $^{35}Cl^-$ NMR transition is typically over 10^4 times larger for chloride bound to a macromolecule than for chloride in solution (17, 18). As a result, when chloride exchanges sufficiently rapidly between binding sites and solution, the observed line width is larger than that of pure solution chloride. In "Appendix II" we present a detailed analysis of the observed $^{35}Cl^-$ NMR resonance and of the physical processes that cause the line width increase.

The Information Contained in the $^{35}Cl^-$ Line Broadening—The line width increase (or line broadening) contains a variety of information about the sites that give rise to it, as shown in the following simple theoretical analysis. The $^{35}Cl^-$ line broadening (δ) is defined as.

$$\delta = \Delta\nu_{1/2} - (\Delta\nu_{1/2})_F \quad (1)$$

Here $(\Delta\nu_{1/2})_F$ is the line width (at half-height) of free chloride in solution, obtained using a blank sample, and $\Delta\nu_{1/2}$ is the observed line width when binding sites are present. In the presence of a heterogeneous population of independent sites the line broadening may be written ("Appendix II"):

$$\delta = \sum_i \alpha_i \frac{[X_iCl]}{[Cl_T^-]} \quad (2)$$

Here $[Cl_T^-]$ is the total (stoichiometric) chloride concentration, $[X_iCl]$ is the concentration of chloride bound to the ith type of site, and α_i is a proportionality constant. Two fundamental assumptions have been made during the derivation of Equation 2 ("Appendix II," also Refs. 31 and 32). First, it is assumed that the free chloride ions in solution are in vast molar excess relative to the bound chloride ions. This assumption is justified in the experiments presented here because the protein concentration is small: the ratio of band 3,

the most abundant polypeptide in the ghost membrane (33), to the total chloride concentration is always $<10^{-4}$. Second, it is assumed that the only significant pathway available to a bound chloride ion is return to the solution. Here chloride bound to band 3 can undergo translocation as well as dissociation, but the dissociation rate is very fast[3] relative to the translocation rate (turnover rate 400/s at 0 °C (22)); thus, the use of Equation 2 is valid in the system at hand.

An important feature of Equation 2 is that the observed line broadening is the sum of the additive contributions from the different types of sites:

$$\delta = \sum_i \delta_i \tag{3}$$

where δ_i ($= \alpha_i\,[X_iCl]/[Cl_T]$) is directly proportional to the fraction of total chloride that is bound to the ith type of site. This relationship can be rewritten in terms of bulk parameters to yield the desired final result. The quantity $[X_iCl]$ can be replaced using the expression $[X_iCl]/[X_{T_i}] = [Cl_F^-]/([Cl_F^-] + K_{D_i})$, where $[X_{T_i}]$ is the total (stoichiometric) concentration of the ith type of site, $[Cl_F^-]$ is the free chloride concentration, and K_{D_i} is the chloride dissociation constant for the ith type of site. In addition, the quantity $[Cl_F^-]$ is essentially equivalent to $[Cl_T^-]$ since it is assumed that the free chloride ions are in vast molar excess to the bound chloride ions. Substitution for $[X_iCl]$ in Equation 2 gives

$$\delta = \sum_i \cdot \alpha_i \frac{[X_{T_i}]}{[Cl^-] + K_{D_i}} \tag{4}$$

where we now write $[Cl_T^-]$ simply as $[Cl^-]$. Finally, $[X_{T_i}]$ can be expressed in terms of the total ghost protein concentration [P], using the simple proportionality $[X_{T_i}] = Z_i[P]$

$$\delta = [P] \cdot \sum_i \alpha_i \frac{Z_i}{[Cl^-] + K_{D_i}} \tag{5}$$

where Z_i is a proportionality constant.

Equation 5 indicates that the quantity $\delta/[P]$ contains all of the interesting information provided by the assay (Hereafter line broadenings will generally be expressed in the units of hertz per mg/ml of total ghost protein.) The information contained in the quantity α_i depends on the rate of chloride exchange between the ith type of site and solution: in the rapid exchange limit α_i depends upon the characteristics of the binding site environment, while in the slow exchange limit α_i depends upon the rate constant for chloride dissociation from the site ("Appendix II"). The proportionality constant Z_i contains information on the number of sites of the ith type. If a particular protein P_i possesses the ith type of site, then Z_i can be written

$$Z_i = n_i \cdot [P_{T_i}]/[P] \tag{6}$$

For the ghost membrane system the n_i have not yet been determined because the α_i are presently unknown. Nevertheless, the line broadening remains a useful assay for chloride binding sites because of the linear relationship between the line broadening and the binding site concentration (Equation 4). The line broadening also contains information on the chloride dissociation constant of each type of site. It is convenient to recast Equation 5 in terms of the inverse chloride concentration to emphasize the high affinity chloride binding sites:

$$\frac{\delta}{[P]} = \sum_i \frac{\alpha_i \cdot Z_i}{K_{D_i}} \cdot \frac{[Cl^-]^{-1}}{[Cl^-]^{-1} + K_{D_i}^{-1}} \tag{7}$$

[3] J. J. Falke, R. J. Pace, and S. I. Chan, unpublished data.

or, for a single type of site:

$$\frac{\delta_i}{[P]} = \frac{\alpha_i \cdot Z_i}{K_{D_i}} \cdot \frac{[Cl^-]^{-1}}{[Cl^-]^{-1} + K_{D_i}^{-1}} \tag{8}$$

This equation states that a high affinity site ($K_{D_i} \lesssim [Cl^-]$) will give rise to a square hyperbola on a plot of line broadening *versus* $[Cl^-]^{-1}$, while on the same plot the curve due to a low affinity site ($K_{D_i} \gg [Cl^-]$) collapses to a straight line of zero slope. Consequently, binding sites can be operationally defined as high or low affinity sites on the basis of their behavior in this type of plot.

Experimental Justification of the $^{35}Cl^-$ Line Broadening Assay for Chloride Binding Sites—The preceding theoretical analysis of the chloride binding assay is supported experimentally by the data of Fig. 3, which demonstrates that at constant $[Cl^-]$ the $^{35}Cl^-$ line broadening is directly proportional to the concentration of chloride binding sites on leaky ghost membranes. This simple linear relationship enables straightforward examination of the leaky ghost system, where the assay reveals a variety of important binding site characteristics.

The Line Broadening Due to DNDS-sensitive Sites—Multiple types of chloride binding sites exist on leaky ghost membranes, since many composite proteins are present (34, 35). The $^{35}Cl^-$ line broadening contributions of the different types of sites are additive (Equation 3); thus, the line broadening due to band 3 transport sites can be identified using a competitive inhibitor which blocks the binding of chloride to the transport sites, for example DNDS.

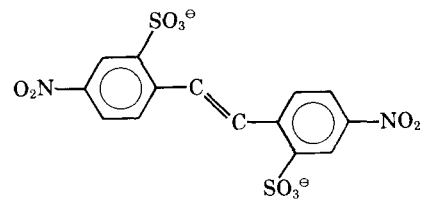

This molecule is a potent anion exchange inhibitor that binds

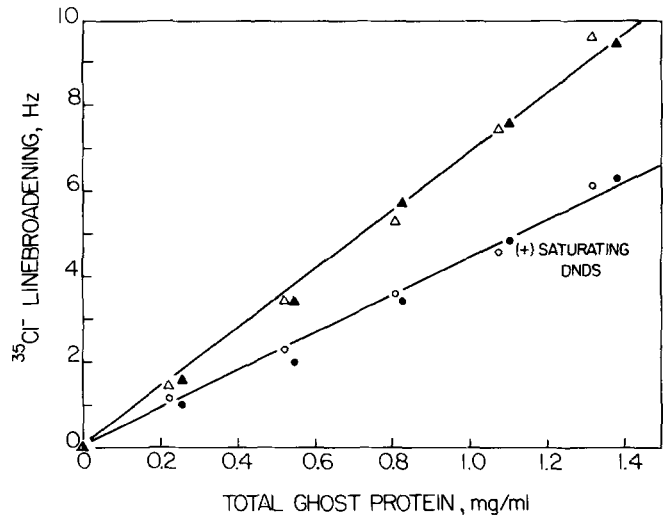

FIG. 3. The relationship between the $^{35}Cl^-$ line broadening and the ghost membrane concentration. The $^{35}Cl^-$ line broadening of samples containing leaky ghost membranes with (●, ○) or without (▲, △) DNDS, 1 mM total concentration. The *solid lines* are least squares best fit straight lines ($y = Mx$) that have slopes of 6.87 ± 0.04 Hz/mg/ml of total ghost protein and 4.41 ± 0.04 Hz/mg/ml of total ghost protein. The buffers used were: 250 mM NH_4Cl, 5 mM NaH_2PO_4, 20% D_2O, pH to 8.0 with NH_4OH (▲, ●); or 220 mM NaCl, 30 mM glycylglycine HCl, 2.5 mM NaH_2PO_4, 20% D_2O, pH to 8.0 with NaOH (△, ○). Spectral parameters: 8.8 MHz, 3 °C, and standard assay parameters (see text).

reversibly to the extracellular band 3 anion transport sites in a manner that prevents chloride binding (1, 28, 36).

A saturating concentration (or, a concentration sufficient to yield maximal inhibition, see Fig. 4) of DNDS partially reduces the ghost line broadening (Fig. 3); the line broadening of DNDS-saturated membranes is 4.41 ± 0.04 Hz/mg/ml of total protein, which is 36% less than the value for DNDS-free ghosts of 6.87 ± 0.04 Hz/mg/ml. Thus, at least two types of chloride binding sites exist on ghost membranes. The sites that give rise to the DNDS-sensitive component of the line broadening are termed the DNDS-sensitive sites, while the remaining sites are DNDS-insensitive. The additivity of line broadening enables isolation of the DNDS-sensitive line broadening by subtraction of the DNDS-insensitive line broadening from the total line broadening. This DNDS subtraction technique will often be used in future presentations of data.

DNDS Binds to Band 3 Transport Sites and Thereby Inhibits the $^{35}Cl^-$ Line Broadening—The line broadening of the DNDS-sensitive sites is inhibited by DNDS binding to a class of inhibitory binding sites that are identical, since the DNDS binding is well described by a single apparent dissociation constant (Fig. 4). This apparent K_D is quantitatively similar to the known apparent K_D for DNDS binding to band 3 transport sites in the presence of 250 mM chloride (Table I). Note that because of the presence of chloride, which competes with DNDS for binding (data not shown; also Ref. 28), the apparent K_D is larger than the true K_D for DNDS binding to the inhibitory sites ("Appendix III").

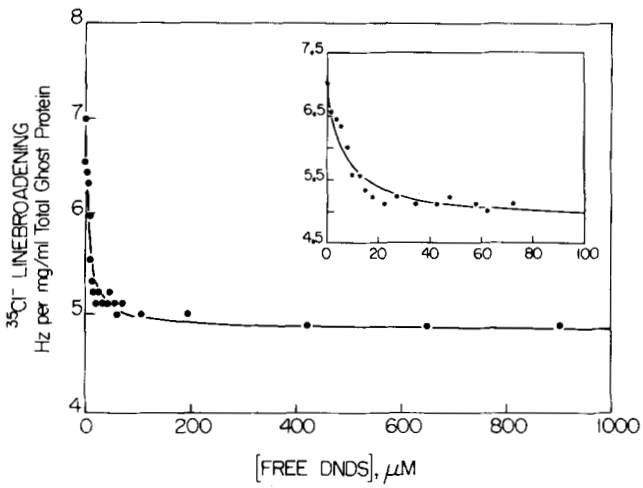

FIG. 4. **The effect of DNDS on the ghost membrane $^{35}Cl^-$ line broadening.** Samples were prepared containing leaky ghost membranes and different concentrations of unbound DNDS. The *solid curve* is the nonlinear least squares best fit curve ($y = A - Bx/(x + K_D)$) for a homogeneous set of sites with an apparent K_D of 6.4 ± 0.5 μM for DNDS binding. The buffer was 250 mM NH_4Cl, 5 mM NaH_2PO_4, 20% D_2O, pH to 8.0 with NH_4OH. Spectral parameters: 8.8 MHz, 3 °C, and standard assay parameters (see text).

TABLE I

Apparent dissociation constants for substrate and inhibitor binding to DNDS-sensitive sites on ghost membranes

Anion	DNDS-sensitive site[a] apparent K_D	Band 3 transport site[b] apparent K_D
Cl^-	80 ± 30 mM	67, 65 ± 5 mM[c]
DNDS[d]	6.4 ± 0.5 μM	4.4 μM[e]

[a] Obtained as described in text.
[b] From equilibrium chloride exchange measurements in red cells.
[c] From Refs. 20 and 38; both have been corrected for the modifier effect.
[d] Both values are given for $[Cl^-]$ = 250 mM.
[e] Extrapolated from Fig. 7 in Ref. 28.

DNDS is known to bind to the extracellular band 3 transport site with a stoichiometry of one molecule of DNDS/band 3 transport unit (28). When DNDS binds to this site, it inhibits the line broadening due to one or more chloride binding sites (Figs. 3 and 4). The affected sites could include: transport sites on band 3, other chloride binding sites on band 3, or chloride binding sites on a protein(s) other than band 3 that are allosterically coupled to the DNDS binding sites. One parameter which is useful in the identification of the DNDS-sensitive sites is the affinity of these sites for chloride.

The DNDS-sensitive Sites Are High Affinity Chloride Binding Sites—Both high affinity and low affinity chloride binding sites are observed in the leaky ghost membrane system (Fig. 5*A*). In the presence of a saturating concentration of DNDS, the line broadening due to ghost membranes is well approximated by a best fit straight line of zero slope (Fig. 5*A*, *lower curve*). Thus, the DNDS-insensitive sites can be operationally defined as low affinity sites that satisfy $K_{D_i} \gg 0.5$ M. (The plot could not be extended to chloride concentrations greater than 0.5 M because DNDS becomes increasingly insoluble at such chloride concentrations.) In the absence of DNDS, high affinity sites appear (Fig. 5*A*, *upper curve*). The resulting line broadening is the sum of the contributions from both the DNDS-sensitive and insensitive sites. This line broadening is well approximated by a best fit curve calculated for (*a*) a homogeneous set of high affinity binding sites described by Equation 8, plus (*b*) a set of low affinity binding sites described by the best fit straight line obtained for the DNDS-containing samples. The data indicate that saturation with DNDS completely inhibits the line broadening of the high affinity sites but has no effect on the low affinity sites.

The apparent dissociation constant for chloride binding to the high affinity sites can be determined from the best fit curve in Fig. 5*A*. Alternatively, the inverse of the DNDS-sensitive line broadening can be plotted as a function of the chloride concentration (Fig. 5*B*). This type of plot yields a straight line for a homogeneous set of chloride binding sites

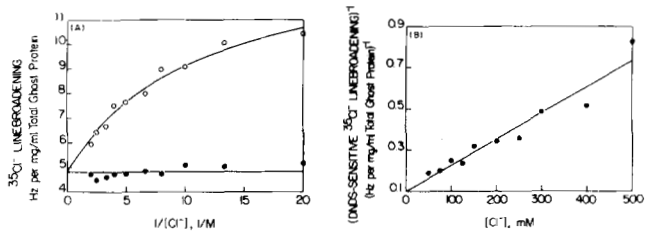

FIG. 5. **The effect of chloride concentration on the ghost membrane $^{35}Cl^-$ line broadening.** *A*, the $^{35}Cl^-$ line broadenings of samples containing leaky ghost membranes with (●) or without (○) DNDS, 1 mM total concentration. The *solid curves* are nonlinear least squares best fit curves calculated for a set of low affinity (lower curve, $y = A$, $K_D \gg 0.5$ M) chloride binding sites plus a homogeneous set of high affinity (*upper curve*, $y = A + Bx/(x + K_D^{-1})$, $K_D = 90 \pm 10$ mM) chloride binding sites. Each sample contained the indicated $[NH_4Cl]$ as well as 2.5 mM NaH_2PO_4, 20% D_2O, pH to 8.0 with NH_4OH. Sufficient citric acid (pH to 8.0 with NaOH) was added to bring the ionic strength up to that of the sample containing the highest $[NH_4Cl]$ = 500 mM. Spectral parameters: 8.8 MHz, 3 °C, and specified assay parameters (see text). *B*, the DNDS-sensitive line broadening was obtained from the data in *A* by subtracting each point for a sample containing DNDS from the corresponding (same $[Cl^-]$) point for a sample without DNDS. Then the inverse of the DNDS-sensitive line broadening was taken. The *solid line* is a linear least squares best fit straight line calculated for a homogeneous set of chloride binding sites ($y = A(1 + [Cl^-]/K_D)$, $K_D = 80 \pm 5$ mM).

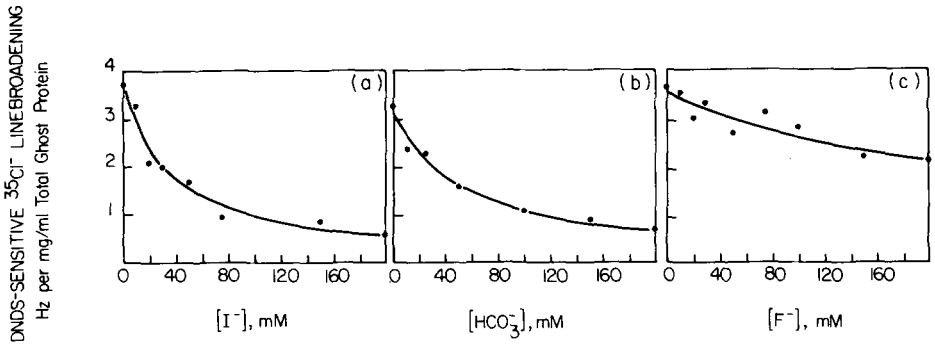

FIG. 6. **The effect of competing anions on the $^{35}Cl^-$ NMR spectrum.** Samples were prepared that contained different concentrations of a competing anion (A^-) and a fixed concentration of chloride (100 mM). The line broadening of a sample containing 1 mM DNDS was subtracted from the line broadening of an otherwise identical DNDS-free sample to yield the line broadening of the DNDS-sensitive sites. The *solid lines* are the nonlinear least squares best fit curves ($y = A - Bx/(x + K_D)$) for a homogeneous set of sites with apparent K_D values of: 34 ± 3 mM for I^- (*a*), 55 ± 4 mM for HCO_3^- (*b*), and 290 ± 30 mM for F^- (*c*). The buffer contained the indicated concentration of NaA as well as 100 mM NaCl, 2.5 mM NaH_2PO_4, 20% D_2O, pH to 8.0 with NaOH. Citric acid (pH to 8.0 with NaOH) was added so that the ionic strength in all samples was the same as that of the [A^-] = 200 mM sample. Spectral parameters: 8.8 MHz, 3 °C and standard assay parameters (see text).

that are described by Equation 8. The extracted best fit apparent K_{D_i}, along with the results of seven similar experiments at 19.6 or 8.8 MHz, together yield an average of 80 ± 30 mM for the apparent K_{D_i} for the chloride binding to the DNDS-sensitive sites. This value is quantitatively similar to the known apparent K_D for chloride binding to band 3 transport sites (Table I).

Surprisingly, no chloride binding sites are observed that have a $K_D \approx 300$ mM, which is the predicted chloride affinity for a site termed the modifier site (1, 20). The existence of a modifier site on band 3 has been proposed to explain the inhibition of chloride self exchange across the membrane which occurs at high [Cl^-]. Such inhibition has been thought to result from chloride binding to the modifier site. Yet no evidence of this chloride binding site is seen in experiments presented here.

The High Affinity Sites Are Band 3 Transport Sites—In order to verify the conclusion that the DNDS-sensitive sites are transport sites and are uncontaminated with modifier sites, we have studied the binding of anions other than chloride to ghost membranes. If an anion (A^-) competes with chloride for binding to an anion binding site, then the $^{35}Cl^-$ NMR assay can be used to study A^- binding. In such an experiment [Cl^-] is held constant, while [A^-] is varied. The resulting data (Fig. 6, for the DNDS-sensitive sites) allow determination of the apparent K_D for A^- binding at the given [Cl^-] (see "Appendix III"). The best fit theoretical curves in Fig. 6 were calculated using the assumption that the DNDS-sensitive sites are a class of identical sites. The reasonable fit of these curves indicates that the assumption of homogeneity is consistent with the data.

The apparent K_D values for bicarbonate, fluoride, chloride, and iodide binding to the DNDS-sensitive sites are given in Table II. Also given are the known apparent K_D values for binding of these anions both to band 3 transport sites and to the hypothetical modifier sites. Note that the apparent K_D values for the DNDS-sensitive sites were obtained in the presence of competing chloride (100 mM), while the other values were obtained in the absence of competing chloride. Two patterns emerge in the data of Table II: (*a*) the apparent K_D values of the DNDS-sensitive sites are larger than the apparent K_D values of band 3 transport sites. This result is expected because only the former values were obtained in the presence of competing chloride. In contrast, the apparent K_D values of the DNDS-sensitive sites are smaller than the apparent K_D values predicted for modifier sites, indicating that the DNDS-sensitive sites have higher affinities for anions than those expected for modifier sites. (*b*) The relative affinities ($I > HCO_3 \gg Cl > F$) exhibited by the DNDS-sensitive sites are essentially the same as those exhibited by band 3 transport sites but are different from those expected for modifier sites. Together the data of Table II suggest that the modifier sites do not contribute significantly to the DNDS-sensitive line broadening. Instead the DNDS-sensitive sites behave like a homogeneous class of band 3 transport sites.

TABLE II

Apparent dissociation constants for anion binding to band 3 sites

Anion	DNDS-sensitive site ([Cl^-] = 100 mM)	Transport site ([Cl^-] = 0 mM)	Modifier site ([Cl^-] = 0 mM)
		mM	
I^-	34 ± 3	10	60
HCO_3^-	55 ± 4	16	565
Cl^-	(190)[c]	67, 65 ± 5[d]	335
F^-	290 ± 30	88	337

[a] Measured as described in text by competing the anion with 100 mM Cl^-.
[b] Obtained from kinetic studies of equilibrium anion exchange in Ref. 20.
[c] Calculated as described in "Appendix III."
[d] From Ref. 38.

DISCUSSION

The $^{35}Cl^-$ NMR line broadening assay reveals two classes of chloride binding sites associated with leaky ghost membranes. The first class consists of low affinity binding sites that are unaffected by DNDS. The second class consists of band 3 transport sites. The line broadening of these transport sites is completely inhibited by a saturating concentration of DNDS. Such line broadening inhibition is consistent with the previous observation that DNDS competes with chloride for binding to the extracellular band 3 transport site (1, 28, 36).

The data presented here indicate that DNDS can be used to isolate that part of the total ghost line broadening which is associated with band 3 transport sites. Actually, DNDS is not very specific for these sites. For instance, we have found that DNDS reduces the line broadening associated with chlo-

ride binding to hemoglobin (data not shown). However, the molar ratio of band 3:hemoglobin in ghosts prepared at pH 8.0 is at least 10:1 (39). This molar ratio would result in a corresponding ratio of DNDS-sensitive line broadenings of at least 100:1 (data not shown), which is a negligible interference. Another protein which could contribute to the DNDS-sensitive line broadening is the erythrocyte Ca^{2+}-ATPase, which is inhibited by 4,4′-diisothiocyanostilbene-2,2′-disulfonate, a structural analogue of DNDS. Again, band 3 is present in great molar excess to this protein; there are ~100 times more copies of band 3 per membrane (40). These examples stress that in the unpurified ghost membrane system, the DNDS-sensitive line broadening could be contaminated with contributions from proteins other than band 3. Fortunately, band 3 is the most abundant polypeptide in ghost membranes (33), so these contaminating contributions could be negligible. This appears to be the case, since the DNDS-sensitive sites are homogeneous with respect to their affinity for a variety of anions (chloride, bicarbonate, fluoride, iodide, and DNDS). Moreover, the apparent affinities that are observed for chloride and DNDS are quantitatively similar to those previously measured for band 3 transport sites. The relative apparent affinities that are observed for the inorganic anions ($I > HCO_3 \gg Cl > F$) are essentially the same as those previously measured for band 3 transport sites. Thus, we believe that the bulk of the sites that make up the DNDS-sensitive class are in fact band 3 transport sites.

An unexpected conclusion of the $^{35}Cl^-$ NMR experiments is that the line broadening assay reveals no evidence for the existence of the proposed inhibitory anion binding site on band 3, which has been termed the modifier site (20). It is possible that this site exists but is invisible to the line broadening assay; a site will become invisible when the quantity α_i is Equation 5 tends to zero. This condition occurs when the exchange of chloride between the binding site and solution is sufficiently slow or when the symmetry of the binding site is tetrahedral or higher.

Actually, we prefer a different explanation in which an inhibitory chloride binding site of the predicted ($K_D \approx 300$ mM) chloride affinity does not exist. Instead inhibition results from nonspecific chloride binding to the low affinity ($K_D \gg 0.5$ M) chloride binding sites that are revealed by the line broadening assay. In this model, bound chloride builds up in the vicinity of the low affinity sites as the chloride concentration increases. The local density of bound chloride ion would in turn inhibit the transport process. The step in the transport cycle which is inhibited is the chloride transmembrane translocation step rather than the chloride binding step, since no inhibition of chloride binding has been observed at chloride concentrations up to 500 mM (Fig. 5). Previous observations indicate that the onset of transport inhibition is rapid as the chloride concentration is increased above 250 mM (41), suggesting that the mechanism of inhibition is highly cooperative.

A cooperative process which could give rise to the observed self inhibition of anion exchange is membrane protein aggregation. Such aggregation has been observed in the erythrocyte system at large [$NaCl^-$] (42). Perhaps in the aggregated state, band 3 cannot undergo a conformational change which is necessary for the transmembrane translocation of bound anion. If aggregation of erythrocyte membrane proteins indeed causes the modifier effect, then a comparison of different anions should show a correlation between the ability of an anion to induce inhibition of band 3 and its ability to induce aggregation of erythrocyte membrane proteins.

In this paper we have used the $^{35}Cl^-$ line broadening assay to observe band 3 transport sites. However, certain questions concerning these sites have not yet been addressed. For instance, do transport sites on both sides of the membrane contribute to the line broadening? If sites on both surfaces are indeed observed, how could DNDS inhibit transport sites on both membrane surfaces when it is thought to bind only to the external transport site? These questions are considered in the following paper.

REFERENCES

1. Knauf, P. A. 91979) *Curr. Top. Membr. Transp.* **12,** 249–363
2. Steck, T. L. (1978) *J. Supramol. Struct.* **8,** 311–324
3. Bennett, V., and Stenbuck, P. J. (1979) *Nature (Lond.)* **280,** 468–473
4. Branton, D., Cohen, C. M., and Tyler, J. (1981) *Cell* **24,** 24–32
5. Cabantchik, A. I., and Rothstein, A. (1974) *J. Membr. Biol.* **15,** 207–226
6. Ho, M. K., and Guidotti, G. (1975) *J. Biol. Chem.* **250,** 675–683
7. Passow, H., Fasold, H., Zaki, L., Schuhman, B., and Lepke, S. (1975) in *Biomembranes: Structure and Function* (Gárdos, G., and Szász, I., eds) FEBS Symposium Series, Vol. 35, pp. 197–214, North-Holland Publishing Co., Amsterdam
8. Gunn, R. B., and Frohlich, O. (1980) in *Membrane Transport in Erythrocytes* (Larsen, V. V., Ussing, H. H., and Wieth, J. O., eds) Vol. 14, pp. 431–449, Munksgaard, Copenhagen
9. Passow, H., Kampmann, L., Fasold, H., Jennings, M., and Lepke, S. (1980) in *Membrane Transport in Erythrocytes* (Larsen, V. V., Ussing, H. H., and Wieth, J. B., eds) Vol. 14, pp. 345–372, Munksgaard, Copenhagen
10. Rothstein, A., Ramjeesingh, M., and Grinstein, S. (1980) in *Membrane Transport in Erythrocytes* (Larsen, V. V., Ussing, H. H., and Wieth, J. B., eds) Vol. 14, pp. 329–344, Munksgaard, Copenhagen
11. Jennings, M. L. (1980) in *Membrane Transport in Erythrocytes* (Larssen, V. V., Ussing, H. H., and Wieth, J. O., eds) Vol. 14, pp. 450–466, Munksgaard, Copenhagen
12. Macara, I. G., and Cantley, L. C. (1981) *Biochemistry* **20,** 5695–5701
13. Wieth, J. O., and Bjerrum, P. J. (1982) *J. Gen. Physiol.* **79,** 253–282
14. Eidelman, O., and Cabantchik, Z. I. (1983) *J. Membr. Biol.* **71,** 141–148
15. Salhany, J. M., and Raunebeuhler, P. B. (1983) *J. Biol. Chem.* **258,** 245–249
16. Lauger, P. (1973) *Biochim. Biophys. Acta* **311,** 423–441
17. Lindman, B., and Forsén, S. (1976) in *NMR: Basic Principles and Progress* (Diehl, P., Fluck, E., Kosfeld, R., eds) Vol. 12, pp. 1–368, Springer-Verlag, NY
18. Forsén, S., and Lindman, B. (1981) *Meth. Biochem. Anal.* 27, 289–486
19. Shami, Y., Carver, J., Ship, S., and Rothstein, A. (1977) *Biochem. Biophys. Res. Commun.* **76,** 429–436
20. Dalmark, M. (1976) *J. Gen. Physiol.* **67,** 223–234
21. Falke, J. J., Pace, R. J., Chan, S. I. (1984) *J. Biol. Chem.* **259,** 6487–6497
22. Frölich, D., and Gunn, R. B. (1981) *Adv. Physiol. Sci.* **6,** 275–280
23. Steck, T. L. (1974) *Meth. Membr. Biol.* **2,** 245–381
24. Fairbanks, G., Steck, T. L., and Wallach, D. F. H. (1971) *Biochemistry* **10,** 2606–2617
25. Farrar, T. C., and Becker, E. D. (1971) *Pulse and Fourier Transform NMR,* pp. 66–85, Academic Press, NY
26. Markwell, M. A., Haas, S. M., Bieber, L. L., and Tolbert, N. E. (1978) *Anal. Biochem.* **87,** 206–210
27. Lowry, O. H., Rosebrough, N. J., Farr, A. L., and Randall, R. J. (1951) *J. Biol. Chem.* **193,** 265–275
28. Frölich, O. (1982) *J. Membr. Biol.* **65,** 111–123
29. Cousin, J. L., and Motais, R. (1979) *J. Membr. Biol.* **46,** 125–153
30. Lieber, M. R., and Steck, T. L. (1982) *J. Biol. Chem.* **257,** 11651–11659
31. McConnell, H. M. (1958) *J. Chem. Physiol.* **28,** 430–431
32. Swift, T. J., and Connick, R. E. (1962) *J. Chem. Physiol.* **37,** 307–320
33. Jones, M. N., and Nickson, J. K. (1981) *Biochim. Biophys. Acta* **650,** 1–20
34. Lux, S. E. (1979) *Nature (Lond.)* **281,** 426–429
35. Haest, C. W. M. (1982) *Biochim. Biophys. Acta* **694,** 331–352
36. Barzilay, M., and Cabantchik, Z. I. (1979) *Membr. Biochem.* **2,** 297–322
37. Deleted in proof
38. Brazy, P. C., and Gunn, R. B. (1976) *J. Gen. Physiol.* **68,** 583–599
39. Shaklai, N., Yguerabide, J., and Ranney, H. M. (1977) *Biochemistry* **16,** 5585–5592
40. Niggli, V., Sigel, E., and Carafoli, E. (1982) *FEBS Lett.* **138,** 164–166
41. Cass, A., and Dalmark, M. (1973) *Nat. New Biol.* **244,** 47–49
42. Elgsaeter, A., and Branton, D. (1974) *J. Cell. Biol.* **63,** 1018–1036
43. Cabantchik, Z. I., Knauf, P., and Rothstein, A. (1977) *Biochem. Biophys. Acta* **515,** 239–302
44. Vaughan-Jones, R. D. (1982) *Philos. Trans. R. Soc. Lond. B Biol. Sci.* **299,** 537–548
45. White, A., Handler, P., and Smith, E. L. (1973) *Principles of Biochemistry,* 5th Ed, McGraw-Hill Publications, Minneapolis, MN
46. Lehninger, A. L. (1975) *Biochemistry,* 2nd Ed, pp. 789–793, Worth, New York
47. Falke, J. J. (1984) Ph.D. dissertation, California Institute of Technology

Supplementary Material to

CHLORIDE BINDING TO THE ANION TRANSPORT BINDING SITES OF BAND 3: A ^{35}Cl NMR STUDY

Joseph J. Falke, R. J. Pace, and Sunney I. Chan

APPENDIX I. THE RATE OF ION FLOW THROUGH THE BAND 3 TRANSPORT SYSTEM

Due to the importance of band 3 in the respiration of CO_2, this protein is present in large quantities in vertebrates. Moreover, the band 3 transport unit has evolved a rapid turnover rate. As a result, the vertebrate band 3 system is a major ion transport pathway. The other most heavily used ion transport pathway in vertebrates is the H^+-ATPase, which supplies ATP to all active transport systems as well as to many other metabolic pathways. Sufficient information exists on the human system to compare the rate of ion flow through the band 3 and H^+-ATPase systems.

Although band 3 may be found in a variety of cell types (1,43,44), only band 3 in red cells will be considered here. In this case the total flow of anions through the entire population of band 3 transport units possessed by an individual human is $\geq 8 \times 10^{23}$ ions/sec (calculated assuming ≥ 5 l of blood per individual (45), 3.2×10^9 red cells per ml of blood (23), 10^6 band 3 transport units per red cell (1), and 5×10^4 turnovers per sec per transport unit (1)).

An upper limit on the flow of protons through the H^+-ATPase can be calculated by assuming that the energy uptake of an individual is completely converted to ATP. In this case the flow of protons through the H^+-ATPase system is $\leq 4 \times 10^{22}$ ions/sec (calculated assuming an energy intake of 3000 kcal per individual per day (45), an energy expenditure of ≥ 10 kcal per mole of ATP synthesized under physiological conditions (45), and a transport of 2 protons per molecule of ATP synthesized (46). The upper limit proton flow of $\leq 4 \times 10^{22}$ ions/sec is actually an average flow which might be smaller than the peak flow achieved during peak metabolic performance. However, this average flow is at least 20 times slower than the average flow of anions through the band 3 system. Thus, the band 3 system, at least on the average, is the most heavily used ion transport system in a typical vertebrate animal.

APPENDIX II. THE EFFECT OF BINDING SITES ON THE ^{35}Cl NMR RESONANCE

The ^{35}Cl NMR spectrum of free chloride solution is a simple one that contains a single resonance of Lorentzian shape. In contrast, the spectrum of chloride bound to macromolecular binding sites can be quite complex, and some of this complexity can appear in the spectrum of chloride which is exchanging between binding sites and solution. The following analysis shows, however, that in a typical $^{35}Cl^-$ linebroadening experiment of the type conducted here, the observed spectrum is essentially the simple spectrum of solution chloride except that the linewidth can be increased by the presence of the binding sites. We shall also derive the quantitative relationship between the $^{35}Cl^-$ linebroadening and the concentration of chloride binding sites. These results can be generalized to describe any spin = 3/2 nucleus.

The $^{35}Cl^-$ NMR Resonance in the Absence of Chemical Exchange

The oriental crystal case. The ^{35}Cl nucleus (S = 3/2) possesses a quadrupole moment and also gives rise to three distinct NMR transitions. The interaction of the quadrupole moment with the electric field gradient at the nucleus largely determines the characteristics of the $^{35}Cl^-$ NMR spectrum. In the following discussion it is assumed that the electric field gradient has cylindrical symmetry, as is generally the case for a single chloride-ligand bond. In an oriented crystal all three transitions can be observed as separate resonances (Figure A1) where the splitting Δ_1 is given by:

$$\Delta_1 = \left|\chi \cdot \frac{\pi}{2} \cdot (3\cos^2\theta - 1)\right| \qquad \text{(A1)}$$

Here χ is the quadrupolar coupling constant for chloride in the crystal environment and θ is the angle between the direction of the static magnetic field and the principal axis of the electric field gradient at the nucleus. The central transition possesses 40% of the integrated intensity and the two equivalent flanking transitions each possess 30%. The linewidths of the flanking transitions are the same and are larger than that of the central resonance.

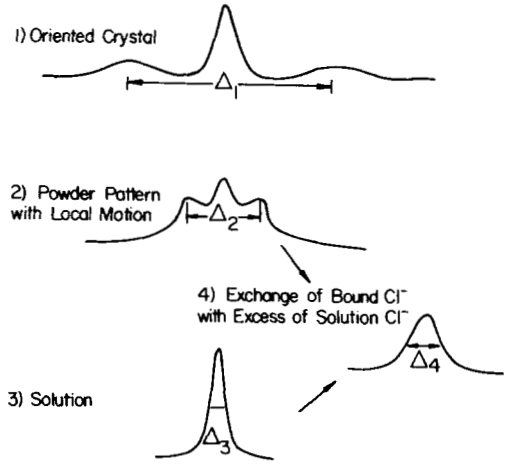

Figure A1. The $^{35}Cl^-$ NMR spectrum in four different environments.

The solution case. In contrast to the spectrum of chloride in a crystal, the spectrum of pure solution chloride is simplified by rapid, unrestricted tumbling. Such tumbling over all angles θ averages the quadrupolar splitting (Equation A1) to zero. The tumbling is also sufficiently isotropic to eliminate the differences in linewidth for the different transitions. Thus, the transitions have the same resonance frequency and linewidth and they sum to give a single Lorentzian line (Figure A1 and text Figures 1,2).

The membrane bound case. The spectrum of chloride bound to membrane-associated protein binding sites combines elements of both the crystal and solution chloride cases. A membrane protein tumbles sufficiently slowly that a specific binding site orientation gives rise to a bound chloride spectrum similar to that of the oriented crystal case (Figure A1, Equation A1). However, motional averaging, restricted to certain directions, may also be present. Restricted but rapid local motions in chloride binding sites have been proposed to explain unexpectedly small quadrupolar effects in a variety of protein systems (18). When such motions are present, they reduce the quadrupolar splitting (Equation A1) observed for a particular average orientation of the binding site. Thus, the quadrupolar splitting becomes

$$\Delta_1 = \left|\chi \cdot \frac{\pi}{2} \cdot (3\cos^2\theta - 1) \cdot S\right| \qquad \text{(A2)}$$

where the order parameter S can have the values $0 \leq |S| \leq 1$. Equation A2 can be applied, for instance, to chloride binding to sites on ghost membranes. In this system the chloride binding sites are randomly oriented so that the spectrum of membrane-bound chloride is a superposition of spectra for all average orientations. The resulting spectrum is a powder pattern (Figure A1) where the splitting Δ_2 is given by:

$$\Delta_2 = \left|\chi \cdot \frac{\pi}{2} \cdot S\right| \qquad \text{(A3)}$$

The maximum splitting is achieved only when the order parameter $|S|$ attains its maximum value of unity. If the bound chloride experiences rapid local motion, the order parameter becomes $0 \leq |S| < 1$. In the limit of sufficiently rapid, unrestricted motion the order parameter becomes $|S| = 0$, and the observed spectrum collapses to a single line, as for solution chloride.

The Effects of Chemical Exchange on the $^{35}Cl^-$ NMR Resonance

The transverse relaxation rate of chloride undergoing exchange. The transverse relaxation rate ($1/T_2$) of an NMR transition is the rate at which its transverse (perpendicular to the static magnetic field) magnetization decays to the equilibrium value of zero. This relaxation process determines the linewidth of the transition and thus measurably affects the shape of the NMR spectrum. For the application at hand, the linebroadening of the observed $^{35}Cl^-$ resonance is best understood in terms of the effect of binding sites on the transverse relaxation rates of the three distinct $^{35}Cl^-$ NMR transitions.

In the experiments presented here (see Results) the observed $^{35}Cl^-$ NMR resonance is dominated by the contribution from solution chloride ions. Using McConnell's modified Bloch equations for chemical exchange (31), Swift and Connick have treated the exchange problem for the case in which the unbound species is in vast molar excess relative to the bound species (32). If the process of exchange between the bound and free states does not itself induce transitions between spin states, then the Swift and Connick results can be applied to the three $^{35}Cl^-$ NMR transitions by treating each transition separately. Consider a set of identical binding sites that have different average orientations and therefore different average values of the angle θ. For the n'th transition, the transverse relaxation rate observed for solution chloride ions in the presence of the binding sites is:

$$\frac{1}{T_{2_n}} = \frac{1}{T_{2F}} + \frac{1}{\tau_{FB}} \cdot \sum_\theta p_\theta \cdot \frac{\left(\frac{1}{T_{2B_n}^2} + \Delta\omega_{n,\theta}^2\right) + \frac{1}{T_{2B_n} \cdot \tau_{BF}}}{\left(\frac{1}{T_{2B_n}^2} + \Delta\omega_{n,\theta}^2\right) + \frac{2}{T_{2B_n} \cdot \tau_{BF}} + \frac{1}{\tau_{BF}^2}} \qquad \text{(A4)}$$

where $1/T_{2F}$ and $1/T_{2B}$ are the transverse relaxation rates of free and bound chloride, respectively; τ_{xy} is the lifetime of chloride in state x before returning to state y; p_θ is the fraction of sites that have a particular value of θ; and $\Delta\omega_\theta$, which depends upon θ, is the difference between the resonance frequencies of free and bound chloride. Equation A4 assumes that the only pathway available to the bound species is dissociation from the site and return to the solution. As shown in the text (see Results), this assumption is reasonable in the band 3 system. An equation analogous to Equation A4 can be derived for a set of heterogeneous binding sites (32).

It is convenient to recast Equation A4 in terms of familiar rate constants and concentrations. First note that the characteristic time (τ_{FB}) spent by a chloride ion in solution before it binds, which can be expressed in terms of the on-rate for binding, can also be related to the off-rate via detailed balancing:

$$\frac{1}{\tau_{FB}} = \frac{\text{ON-RATE}}{[Cl]_F} = \frac{\text{OFF-RATE}}{[Cl]_F} = k_{OFF} \cdot \frac{[X\text{-}Cl]}{[Cl]_F} = \frac{p_B}{\tau_{OFF}} \qquad \text{(A5)}$$

Here $[Cl]_F$ is the free chloride concentration, $[X\text{-}Cl]$ is the bound chloride concentration, and k_{OFF} is the rate constant for dissociation. The quantity $p_B = [X\text{-}Cl]/[Cl]_F$ is essentially the fraction of total chloride which is bound to the site, since it is assumed $[Cl]_F = [Cl]_T$, where $[Cl]_T$ is the total stoichiometric chloride concentration. Similarly, the characteristic time (τ_{BF}) spent by a chloride ion in the binding site before it leaves can be expressed in terms of the off-rate:

$$\frac{1}{\tau_{BF}} = \frac{\text{OFF-RATE}}{[X\text{-}Cl]} = k_{OFF} = \frac{1}{\tau_{OFF}} \qquad \text{(A6)}$$

Substitution of Equations (A5) and (A6) into (A4) yields the desired expression:

$$\frac{1}{T_{2_n}} = \frac{1}{T_{2F}} + \frac{p_B}{\tau_{OFF}} \sum_\theta p_\theta \frac{\left(\frac{1}{T_{2B_n}^2} + \Delta\omega_{n,\theta}^2\right) + \frac{1}{T_{2B_n} \cdot \tau_{OFF}}}{\left(\frac{1}{T_{2B_n}^2} + \Delta\omega_{n,\theta}^2\right) + \frac{2}{T_{2B_n} \cdot \tau_{OFF}} + \frac{1}{\tau_{OFF}^2}} \qquad \text{(A7)}$$

This expression defines the linewidth ($= 1/\pi T_{2_n}$) of the n'th transition and is easily examined in the limits of slow and rapid exchange.

The slow exchange case. Here the bound and free chloride give rise to separate spectra. In general, only the free chloride spectrum is observed (see text), yet the binding sites can have an effect on the linewidth of the free chloride spectra. In order for the slow exchange limit to pertain, complete dephasing of the transverse magnetization must occur during a single visit by a chloride ion to a binding site. Moreover, this condition must be satisfied for all three transitions.

Complete dephasing of the transverse magnetization will occur upon binding if the intrinsic transverse relaxation time of the bound chloride (T_{2B_n}) is small compared to the lifetime of the chloride ion in the site. When this conditions holds so that terms containing $1/\tau_{OFF}$ can be neglected in Equation A7, one obtains

$$\frac{1}{T_{2_n}} = \frac{1}{T_{2F}} + \frac{p_B}{\tau_{OFF}} = \frac{1}{T_{2F}} + R_{EX} \qquad \text{(A8)}$$

where R_{EX} is the additional or excess relaxation rate relative to that of free chloride. When $T_{2B_n} \ll \tau_{OFF}$ so that Equation A8 holds for each transition, the binding equilibrium is in the slow exchange limit.

Since for slow exchange complete dephasing occurs during a single visit to a binding site, the excess relaxation rate is simply a consequence of the on-reaction. Thus, it is not surprising that the excess relaxation rate from Equation A8 is the same as the on-rate for the binding of a chloride ion to a binding site ($1/\tau_{FB} = p_B/\tau_{OFF}$, Equation A5). Note that R_{EX} is the same for all three transitions so that in the slow exchange limit the transitions have the same linewidth ($= 1/(\pi T_{2_n})$). In order for the linewidth of the free chloride to be measurably increased, Equation A8 indicates that R_{EX} must be at least of the same magnitude as the relaxation rate of pure solution chloride ($1/T_{2F}$). Since we have just shown $R_{EX} = 1/\tau_{FB}$, the required condition for measurable linebroadening can be restated: sufficient probability must exist that a free chloride ion in solution will visit a binding site before complete dephasing occurs in solution.

These results allow description of the form of the observed $^{35}Cl^-$ NMR spectrum for the slow exchange case. As in the case of pure solution chloride the three transitions have identical linewidths. Moreover, since bound chloride does not contribute to the observed spectrum, there is no quadrupolar splitting nor any shift in the resonance frequency. Instead, the observed spectrum is a single Lorentzian line centered at the pure solution chloride resonance frequency. If the on-rate for binding is sufficiently large, then the observed linewidth will be larger than the pure solution chloride linewidth by the amount $p_B/(\pi \cdot \tau_{OFF}) = (k_{OFF} \cdot [X\text{-}Cl])/([Cl]_T \cdot \pi)$. Here the proportionality constant α (see text, Equation 2) is given by $\alpha = k_{OFF}/\pi$.

The rapid exchange case. In the rapid exchange limit each chloride ion visits a large number of binding sites before complete dephasing of the transverse magnetization occurs. The binding sites that a chloride ion visits have different but random average orientations. Thus, one feature of the rapid exchange limit is that the quadrupolar splitting (Figure A1, Equation A3) is essentially averaged to zero, due to the rapid sampling of different binding site orientations that occurs upon successive visits to different sites (pseudo-tumbling).

The observed resonance frequency in the rapid exchange limit is typically similar to, but not identical to, the resonance frequency of solution chloride. If a chemical shift occurs upon binding, all three of the bound chloride resonances are shifted by the same amount and in the same direction. Due to the rapid exchange of chloride ion between the bound and free states, the ion experiences an average environment. As a result, each transition gives rise to a single exchange-averaged resonance rather than separate resonances for bound and free chloride. The three different transitions give rise to three different exchange-averaged resonances that have the same resonance frequency, since pseudo-tumbling averages the quadrupolar splitting to zero. However, the observed exchange-averaged resonance frequency is the weighted average of the central frequencies of the bound and solution

chloride spectra. In particular, the difference between the central frequencies of the exchange-averaged and solution chloride spectra is given by

$$\Delta\omega_{OBS} = p_B \cdot \Delta\sigma \tag{A9}$$

where $\Delta\sigma$ is the difference between the central frequencies of the bound and solution chloride spectra. Equation A9 assumes that the fraction of the total chloride which is bound at any moment satisfies $p_B \ll 1$. This condition is satisfied in the experiments presented here since $p_B \leq 10^{-3}$. The quantity $\Delta\sigma$ is typically in the range 100 - 200 Hz (assuming a resonance frequency of 10 MHz and a chemical shift of 10 - 20 ppm, which has been observed for chloride binding to micelles of alkylammonium ions (17)). For such a case, Equation A9 indicates that the central frequency of the exchange-averaged $^{35}Cl^-$ NMR spectrum will be essentially the same as that of solution chloride.

The transverse relaxation rate for the rapid exchange case can be derived from Equation A7 using the condition $1/\tau_{OFF} \gg 1/T_{2B_n} \cdot |\Delta\omega_{n,\theta}|$, which states that for each transition the off-rate of a bound chloride ion is much larger than both a) the bound chloride transverse relaxation rate, and b) the resonance frequency shift that occurs upon binding. In this limit, Equation A7 becomes

$$\frac{1}{T_{2_n}} = \frac{1}{T_{2F}} + p_B \cdot \tau_{OFF} \cdot \left[\frac{1}{T_{2B_n}^2} + \overline{(\Delta\omega_{n,\theta}^2)} + \frac{1}{T_{2B_n} \cdot \tau_{OFF}} \right] = \frac{1}{T_{2F}} + R_{EX} \tag{A10}$$

where the quantity $\Delta\omega_{n,\theta}^2$ has been averaged over all θ using the weighting function p_θ. According to Equation A10, the excess relaxation rate can be dominated either by $1/T_{2B_n}$ or $\Delta\omega_{n,\theta}$.

In the case $1/T_{2B_n}^2 \geq \overline{(\Delta\omega_{n,\theta}^2)}$ the excess relaxation rate becomes

$$R_{EX} = \frac{p_B}{T_{2B_n}} \tag{A11}$$

where the intrinsic binding site transverse relaxation rate $1/T_{2B_n}$ is dominant. Note that when this relationship holds, the transverse relaxation rate ($= 1/T_{2F} + p_B/T_{2B_n}$) is simply the weighted average of the instrinsic relaxation rates of free and bound chloride ($p_F \approx 1$ due to the vast excess of free chloride). The value of $1/T_{2B_n}$ is the same for the flanking transitions but the central transition can have a $1/T_{2B_n}$ that is smaller. This difference in $1/T_{2B_n}$ between different transitions vanishes in the limit $\omega_n\tau_c \ll 1$ (the extreme narrowing limit) where ω_n is the resonance frequency of the n'th transition and τ_c is the correlation time for isotropic tumbling.

In the case $\overline{(\Delta\omega_{n,\theta}^2)} \gg 1/T_{2B_n}^2, 1/(T_{2B_n} \cdot \tau_{OFF})$, the excess relaxation rate becomes

$$R_{EX} = p_B \cdot \tau_{OFF} \cdot \overline{(\Delta\omega_{n,\theta}^2)} \tag{A12}$$

where the resonance frequency shift $\Delta\omega_{n,\theta}$ that occurs upon binding is dominant. For the flanking transitions, $\Delta\omega_{f,\theta} = \Delta\sigma \pm \Delta_1$, where $\Delta\sigma$ is the resonance frequency shift that occurs upon binding, and Δ_1 is the quadrupolar splitting defined in Equation A2. The quantity of interest $\overline{(\Delta\omega_{f,\theta}^2)}$ can be calculated by averaging over a uniform distribution of θ to yield

$$\overline{(\Delta\omega_{f,\theta}^2)} = \Delta\sigma^2 + \frac{4}{5}(\chi \cdot \frac{\pi}{2} \cdot S^2) \tag{A13}$$

The central transition is unaffected by quadrupolar splitting so that $\Delta\omega_{c,\theta} = \Delta\sigma$, and $\overline{(\Delta\omega_{c,\theta}^2)} = \Delta\sigma^2$. Thus, the quantity $\overline{(\Delta\omega_{n,\theta}^2)}$, which is the same for the flanking transitions, is generally larger for the flanking transitions than for the central transition. However, when the order parameter S becomes zero, the three transitions have the same value of $\overline{(\Delta\omega_{n,\theta}^2)}$.

It is interesting to note that the intrinsic binding site relaxation rate $1/T_{2B_n}$ dominates the excess relaxation rate even when $1/T_{2B_n}^2 = \overline{(\Delta\omega_{n,\theta}^2)}$ (Equation A11). The basis for this dominance becomes obvious when the decay of the transverse magnetization is described in terms of a one-dimensional random walk. The decay of the transverse magnetization is due to fluctuations that, to a first approximation, can be described as random walks in resonance frequency. The intrinsic transverse relaxation of bound chloride is caused by fluctuations in the length and orientation of chloride-ligand bonds. These fluctuations are fast; thus, a large number of random walk steps occur during a single binding site visit. In contrast, in the random walk due to $\Delta\omega_n$ each binding site visit is only a single step. Thus, relaxation due to $\Delta\omega_n$ tends to occur more slowly than that due to the intrinsic $1/T_{2B_n}$.

A measurable increase in the solution chloride linewidth will occur only if the excess relaxation rate is at least the same order of magnitude as the transverse relaxation rate of pure solution chloride (Equation A10). When the inherent binding site transverse relaxation dominates (Equation A11), this condition becomes

$$\frac{1}{T_{2F}} \leq \frac{p_B}{T_{2B_n}} = \frac{\tau_{OFF}}{T_{2B_n}} \cdot \left(\frac{[X\text{-}Cl] \cdot k_{OFF}}{[Cl]_F} \right) \tag{A14}$$

When the frequency shift that occurs upon binding dominates (Equation A12), the condition becomes

$$\frac{1}{T_{2F}} \leq p_B \cdot \tau_{OFF} \cdot \overline{(\Delta\omega_{n,\theta}^2)} = \tau_{OFF}^2 \cdot \overline{(\Delta\omega_{n,\theta}^2)} \cdot \left(\frac{[X\text{-}Cl] \cdot k_{OFF}}{[Cl]_F} \right) \tag{A15}$$

Recall that in the rapid exchange limit the conditions τ_{OFF}/T_{2B_i}, $\tau_{OFF}^2\overline{(\Delta\omega_{n,\theta}^2)} \ll 1$ both hold. Thus, measurable broadening is observed only when each chloride ion makes a large number of binding site visits on the timescale of T_{2F}. This is necessary because each binding site visit only slightly dephases the transverse magnetization of the spin.

In summary, the presence of binding sites can alter significantly the ^{35}Cl NMR resonance of solution chloride when the exchange of chloride between binding sites and solution is in the rapid exchange limit. In this limit the three transitions have the same exchange-averaged resonance frequency which differs negligibly from the resonance frequency of solution chloride. However, the linewidths $(\pi \cdot T_{2_n})^{-1}$ of the three transitions can be significantly different; in particular, the linewidths of the flanking transitions can be larger than that of the central transition. As a result the exchange-averaged $^{35}Cl^-$ NMR resonance is generally a superposition of two Lorentzians: the broader one stems from the flanking transitions and possesses 60% of the total integrated intensity, while the narrower one stems from the central transition and possesses 40% of the total integrated intensity. In certain cases the difference in linewidth between the two Lorentzians is insignificant so that the observed resonance is well approximated by a Lorentzian curve with a single linewidth. Then, from Equations A11 and A12 the linebroadening is: $p_B \cdot (\pi \cdot T_{2B})^{-1}$ when the intrinsic binding site transverse relaxation dominates; or $p_B \cdot \tau_{OFF} \cdot \Delta\omega^2/n$ when the binding site frequency shift dominates. It follows that the proportionality constant α (see text, Equation 2) is either $(\pi \cdot T_{2B})^{-1}$ or $\tau_{OFF} \cdot \Delta\omega^2/n$, respectively.

The case of simultaneous rapid and slow exchange. We have shown elsewhere (47) that the linebroadening due to leaky ghost membranes stems both from sites that are near the rapid exchange limit and from sites that are near the slow exchange limit. In such a system a typical chloride ion will visit many rapidly exchanging sites before it visits a single slowly exchanging site. This follows from the fact that a typical chloride ion must visit many rapidly exchanging sites during the time T_{2F} in order for significant linebroadening to result. In contrast, a typical ion need visit only one or a few slowly exchanging sites during the time T_{2F} in order for significant linebroadening to result. Since visits to slowly exchanging sites are rare while visits to rapidly exchanging sites are frequent, extensive exchange-averaging of the chloride ion environment occurs before a visit to a slowly exchanging site causes complete transverse dephasing. In this case the resonance frequency of the observed $^{35}Cl^-$ NMR resonance is essentially the same as the exchange-averaged resonance for solution chloride in the presence of the rapidly exchanging sites. The slowly exchanging sites do not affect the observed resonance frequency because the chloride ions bound to these sites give rise to a distinct $^{35}Cl^-$ NMR spectrum which is not observed (see Results).

The slowly exchanging sites can, however, measurably increase the transverse relaxation rates for the three $^{35}Cl^-$ NMR transitions. For a homogeneous set of rapidly exchanging sites plus a homogeneous set of slowly exchanging sites, the transverse relaxation rate is equal to the transverse relaxation rate in the rapid exchange case (Equation A10) plus an extra term corresponding to the on-rate for a chloride ion binding to a slowly exchanging site (p_B/τ_{OFF}, Equation A8). Since the excess relaxation rate due to the rapidly exchanging sites is generally different for the flanking and central transitions, the observed resonance is generally a superposition of two Lorentzians that possess 60% and 40% of the total integrated intensity, respectively. However, when the linewidths of the two Lorentzians are sufficiently similar, the observed resonance becomes indistinguishable from a single Lorentzian. For instance, there are rapidly exchanging sites present in a suspension of leaky ghost membranes (47); thus, the observed $^{35}Cl^-$ NMR resonance (Figure 1 in text) is probably a double Lorentzian. Indeed the lineshape is well approximated by a best-fit double Lorentzian where the two linewidths differ by a factor of 2.0 (Figure A2, dashed line). However, the lineshape is also well approximately by a single Lorentzian (Figure 2A, solid line), and for simplicity of data analysis the resonance can be treated as a Lorentzian line that can be described by a single linewidth.

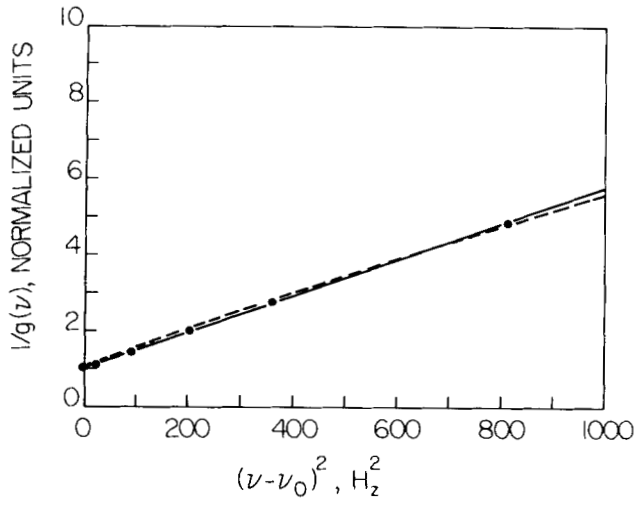

Figure A2. Shown are the data for leaky ghosts from Figure 2 in the text.

APPENDIX III. INHIBITION OF THE DNDS-SENSITIVE $^{35}Cl^-$ LINEBROADENING BY COMPETITIVE INHIBITORS

The DNDS-sensitive chloride binding sites on leaky ghost membranes are a set of band 3 transport sites that bind a variety of anions (see text). In general, different anions are known to compete with each other for binding to these sites (20). The following analysis studies the effect of a population of competing anions on the $^{35}Cl^-$ linebroadening.

Any acceptable model for the mechanism of band 3-catalyzed chloride exchange must explain the fact that in a variety of experiments the transport sites behave like a population of identical anion binding sites. In the present application, for example, the experimental results are well approximated by theoretical curves generated for a class of identical sites. Using this approach, the fraction of sites that are inhibited by a competitive inhibitor is

$$P_I = \frac{[X \cdot I]}{[X]_T} \tag{A16}$$

where $[X \cdot I]$ is the concentration of the bound inhibitor I whose binding excludes chloride binding, and $[X]_T$ is the total transport site concentration. The total transport site concentration can be written $[X]_T = [X]_F + [X \cdot Cl] + [X \cdot I]$. In addition the concentration of bound chloride ($[X \cdot Cl] = [X]_F \cdot [Cl_F]/K_D$) and the concentration of bound inhibitor ($[X \cdot I] = [X]_F \cdot [I]_F/K_I$) can be written in terms of the dissocation constants K_D and K_I and the free reactant concentrations $[Cl]_F$, $[I]_F$ and $[X]_F$. Substitution of these results into Equation A16 gives

$$P_I = \frac{[I]}{[I] + K_I \cdot (1 + [Cl]/K_D)} \tag{A17}$$

Here the free reactant concentrations have been written simply [I] and [Cl].

The dependence of the linebroadening on [I] can now be determined. The inhibited sites do not contribute to the linebroadening; thus, in the presence of inhibitor the observed linebroadening (δ) is less than its maximum value (δ_0):

$$\delta = \delta_0 - P_I\delta_I \tag{A18}$$

where the quantity δ_I is the inhibitor-sensitive linebroadening. Equations A17 and A18 together yield the standard form of an inhibitory curve in which the apparent K_I is the quantity $K_I(app) = K_I (1 + [Cl]/K_D)$. This apparent dissociation constant is a linearly increasing function of $[Cl^-]$ because chloride ions compete with the inhibitor for binding. As the chloride concentration goes to zero, the apparent dissociation constant becomes K_I. This quantity is the true dissociation constant for inhibitor binding only when the transport sites are identical on the microscopic scale (47).

One of the $K_I(app)$ tabulated in the text deserves special mention--the $K_I(app)$ for chloride binding in the presence of 100 mM competing chloride (Table 2). The tabulated value was calculated from the relation $K_I(app) = K_I(1 + [Cl]/K_D)$ using the measured chloride dissociation constant $K_D = 80$ mM. In this case $K_D = K_I$ and $[Cl] = 100$ mM, so the $K_I(app)$ becomes 180 mM. Note that this calculated value could instead be determined experimentally be fixing the natural abundance chloride concentration at 100 mM and then adding $^{37}Cl^-$ to competitively inhibit the binding of the 100 mM natural abundance chloride. Since $^{37}Cl^-$ is silent in the $^{35}Cl^-$ spectrum, the $^{37}Cl^-$ would behave just like the non-chloride anions that have been studied (text, Figure 6).